

An Estimation of the White Dwarf Mass in the Dwarf Nova GK Persei with NuSTAR Observations of Two States

Yuuki Wada,^{1,2*} Takayuki Yuasa,³ Kazuhiro Nakazawa,¹ Kazuo Makishima,⁴
Takayuki Hayashi,^{5,6} and Manabu Ishida^{7,8}

¹Department of Physics, Graduate School of Science, The University of Tokyo, 7-3-1 Hongo, Bunkyo-ku, Tokyo 113-0033, Japan

²High Energy Astrophysics Laboratory, Nishina Center for Accelerator-Based Science, RIKEN, 2-1 Hirosawa, Wako, Saitama 351-0198, Japan

³55 Devonshire Road 239855, Singapore

⁴MAXI team, RIKEN, 2-1 Hirosawa, Wako, Saitama 351-0198, Japan

⁵Department of Graduate School of Science, Nagoya University, Furo-Cho, Chikusa-ku, Nagoya 464-8602, Japan

⁶Goddard Space Flight Center, National Aeronautics and Space Administration, Greenbelt, MD 20771, USA

⁷Institute of Space and Astronautical Science, Japan Aerospace Exploration Agency, 3-1-1 Yoshinodai, Chuo-ku, Sagami-hara 252-5210, Japan

⁸Department of Physics, Tokyo Metropolitan University, 1-1 Minami-Osawa, Hachioji, Tokyo 192-0397, Japan

Accepted 2017 November 03. Received 2017 October 22; in original form 2017 September 05

ABSTRACT

We report on X-ray observations of the Dwarf Nova GK Persei performed by *NuSTAR* in 2015. GK Persei, behaving also as an Intermediate Polar, exhibited a Dwarf Nova outburst in 2015 March–April. The object was observed with *NuSTAR* during the outburst state, and again in a quiescent state wherein the 15–50 keV flux was 33 times lower. Using a multi-temperature plasma emission and reflection model, the highest plasma temperature in the accretion column was measured as $19.7^{+1.3}_{-1.0}$ keV in outburst and $36.2^{+3.5}_{-3.2}$ keV in quiescence. The significant change of the maximum temperature is considered to reflect an accretion-induced decrease of the inner-disk radius R_{in} , where accreting gas is captured by the magnetosphere. Assuming this radius scales as $R_{\text{in}} \propto \dot{M}^{-2/7}$ where \dot{M} is the mass accretion rate, we obtain $R_{\text{in}} = 1.9^{+0.4}_{-0.2} R_{\text{WD}}$ and $R_{\text{in}} = 7.4^{+2.1}_{-1.2} R_{\text{WD}}$ in outburst and quiescence respectively, where R_{WD} is the white-dwarf radius of this system. Utilising the measured temperatures and fluxes, as well as the standard mass-radius relation of white dwarfs, we estimate the white-dwarf mass as $M_{\text{WD}} = 0.87 \pm 0.08 M_{\odot}$ including typical systematic uncertainties by 7%. The surface magnetic field is also measured as $B \sim 5 \times 10^5$ G. These results exemplify a new X-ray method of estimating M_{WD} and B of white dwarfs by using large changes in \dot{M} .

Key words: stars: dwarf novae – X-rays: individual:GK Persei

1 INTRODUCTION

Cataclysmic Variables (CVs) are close binary systems consisting of a mass-accreting white-dwarf (WD) primary and a mass-donating companion. Gas overflowing from the Roche lobe of the companion accretes onto the WD surface, where gravitational energy of the gas is converted mainly into X-ray emission. CVs hosting a magnetised WD are further classified into “Polars” and “Intermediate Polars” (IPs), in which the WDs have magnetic-field strengths of $B \sim 10^{7-9}$ G and $B \sim 10^{5-7}$ G, respectively.

In an IP, the gas from the companion forms an accretion disk down to a radius R_{in} where the gravity working on

the accreting matter is counter-balanced by the magnetic pressure. Then, the gas is captured by the WD’s magnetosphere, and accretes onto the WD surface to form a pair of accretion columns due to the strong magnetic field. In the accretion columns, the gas is heated to 10^{7-8} K by a standing shock, and lands onto the WD surface after releasing most of its energies into thermal X-rays. If R_{in} is far enough from the WD surface, the temperature T_{s} just below the shock is proportional to the gravitational potential of the WD (Aizu 1973) as

$$kT_{\text{s}} = \frac{3}{8} \mu m_{\text{p}} \frac{GM_{\text{WD}}}{R_{\text{WD}}}, \quad (1)$$

where μ is the mean molecular weight, m_{p} is the proton mass, M_{WD} is the WD mass, and R_{WD} is its radius. Therefore, M_{WD} can be estimated by combining the measured T_{s} with

* E-mail: wada@juno.phys.s.u-tokyo.ac.jp

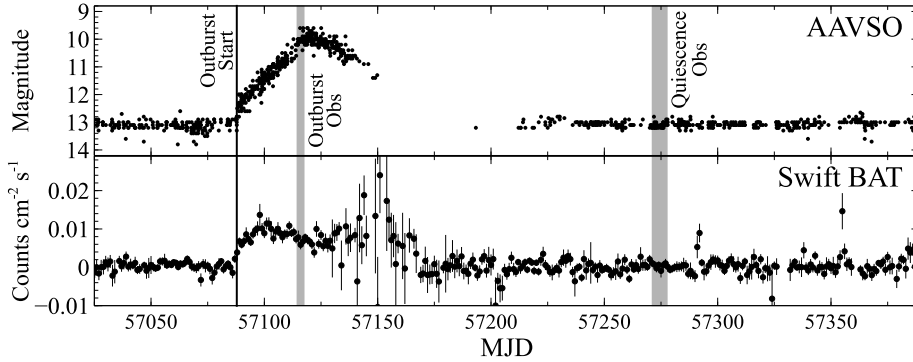


Figure 1. Optical light curves of GK Persei without a filter from AAVSO *International Database*, and the *Swift*/BAT (Krimm et al. 2013) 15–150 keV count rate history from *Swift*/BAT X-ray Transient Monitor web site. The shaded regions indicate the two *NuSTAR* observations.

Table 1. The present observation log of GK Persei by *NuSTAR*.

	Observation ID	Start Date/Time	Stop Date/Time	Exposure ^a	Count rate ^b
Outburst	90001008002	2015-04-04 02:46:07	2015-04-06 15:10:35	42	18.09 ± 0.02
Quiescence	30101021002	2015-09-08 15:46:08	2015-09-11 02:04:09	72	1.080 ± 0.006

^a A net exposure of each of FPMA and FPMB in ks.

^b Averaged 3–50 keV combined count rates of FPMA plus FPMB in units of count s⁻¹.

the standard mass v.s. radius ($M_{\text{WD}}-R_{\text{WD}}$) relation of WDs (Nauenberg 1972)

$$R_{\text{WD}} = 7.8 \times 10^8 \text{ cm} \left[\left(\frac{1.44 M_{\odot}}{M_{\text{WD}}} \right)^{2/3} - \left(\frac{M_{\text{WD}}}{1.44 M_{\odot}} \right)^{2/3} \right]^{1/2}. \quad (2)$$

An X-ray spectrum from an IP is a particular superposition of optically-thin thermal emissions of various temperatures, from T_s downwards (Cropper et al. 1998). To determine T_s , it is hence important to accurately measure both the hard X-ray continuum (e.g. Suleimanov et al. 2005; Yuasa et al. 2010), and the ratio of Fe XXV and XXVI lines at ~ 7 keV (Fujimoto & Ishida 1997). This is because the former is sensitive to the hottest components (with temperature $\sim T_s$), whereas the latter tells us contributions from cooler components arising closer to the WD surface.

GK Persei, at an estimated distance of 477^{+28}_{-25} pc (Harrison et al. 2013a), interestingly exhibits three distinct aspects of CVs; it behaves as an IP, as a Dwarf Nova, and exhibited a classical Nova explosion in 1901 (Williams 1901; Hale 1901). It repeats Dwarf Nova outbursts every 2–3 years, each lasting for 2 months (e.g. Šimon 2002). During outbursts, the optical and X-ray luminosities both increase by a factor of 10–20.

By optical observations, Reinsch (1994) and Morales-Rueda et al. (2002) obtained lower limits of the WD mass in GK Persei as $M_{\text{WD}} \geq 0.78 M_{\odot}$ and $M_{\text{WD}} \geq 0.55 M_{\odot}$ respectively, and upper limits of the inclination angle as $i \leq 73^\circ$ due to lack of eclipses. Through a model fitting to the Nova outburst light curve observed in 1901, Hachisu & Kato (2007) also derived $M_{\text{WD}} = 1.15 \pm 0.05 M_{\odot}$. Ezuka & Ishida (1999) and Suleimanov et al. (2005) measured the shock temperature in outbursts, and derived $M_{\text{WD}} = 0.52^{+0.34}_{-0.16} M_{\odot}$ with *ASCA* and $M_{\text{WD}} = 0.59 \pm 0.05 M_{\odot}$ with *RXTE*, respectively.

However, Suleimanov et al. (2005) pointed out that the WD mass based on the outburst observation could be underestimated by at least 20%. In fact, accretion onto the WD can occur only if R_{in} is smaller than the co-rotation radius, defined as

$$\frac{R_{\Omega}}{R_{\text{WD}}} = 2.3 \left(\frac{P}{1 \text{ min}} \right)^{2/3} \left(\frac{M_{\text{WD}}}{M_{\odot}} \right)^{1/3} \left(\frac{R_{\text{WD}}}{10^9 \text{ cm}} \right)^{-1} \quad (3)$$

(e.g. Warner 1995), where the Keplerian rotation period is equal to the spin period P . When $P = 351$ sec of GK Persei (e.g. Watson et al. 1985) and $M_{\text{WD}} \sim 0.8 M_{\odot}$ are employed, $R_{\text{in}} < R_{\Omega} \sim 10 R_{\text{WD}}$ should be required even in quiescence. Therefore, the condition $R_{\text{in}} \gg R_{\text{WD}}$ may not generally hold, particularly in outbursts. Actually, Brunschweiler et al. (2009) utilised the *Swift*/BAT survey data during quiescence and obtained $M_{\text{WD}} = 0.90 \pm 0.12 M_{\odot}$, which is higher than the estimates from the past X-ray results in outbursts.

A recent outburst from GK Persei started in March 2015, and continued for 2 months (Wilber et al. 2015). During this outburst, Zemko et al. (2017) triggered a Target of Opportunity (ToO) observation with *NuSTAR* and measured a high spin modulation even in a hard X-ray range. Suleimanov et al. (2016) also analysed the ToO data and constrained the WD mass as $M_{\text{WD}} = 0.86 \pm 0.02 M_{\odot}$. The onset of this outburst was serendipitously caught by *Suzaku*, and the obtained data allowed Yuasa et al. (2016) to study the accretion geometry at the beginning of the outburst.

With *NuSTAR*, we observed GK Persei again, after the object returned to its quiescence. Although previous observations of the object in quiescence were unable to detect the hard X-ray component, the high sensitivity of *NuSTAR* has for the first time allowed us to detect its hard X-rays (typically in energies above ~ 20 keV) in quiescence. The present

paper describes a combined analysis of the outburst and quiescence data from *NuSTAR*, and presents a new method to determine R_{in} , M_{WD} , and B of the WD in GK Persei utilising the large change in \dot{M} .

2 OBSERVATIONS AND DATA REDUCTION

The 2015 outburst of GK Persei started on 2015 march 6.84 UT (Wilber et al. 2015). As shown in Figure 1, the ToO observation with *NuSTAR* (Harrison et al. 2013b) was conducted in the middle of the outburst from 2015 April 4 02:46:07 to April 6 15:10:35. The net exposures of FPMA and FPMB are 42 ks each. The second *NuSTAR* observation, in quiescence, was performed from 2015 September 8 15:46:08 to September 11 02:04:09 with a net exposures of 72 ks. The log of the two observations is given in Table 1.

We utilised the data analysis software package **HEASOFT** version 6.20 and a detector calibration database **NuSTAR CALDB** version 20170222, both released and maintained by HEASARC at NASA Goddard Space Flight Center. Photon events in the data sets were extracted with an exclusive data reduction software for *NuSTAR* “**nupipeline**” version 0.4.6 and “**nuproducts**” version 0.3.0. The on-source events were accumulated from a circular region with a radius of $150''$ (in outburst) and $80''$ (in quiescence) centred on the source. The background data were accumulated over a region outside a circle of radius of $170''$ and $100''$ in outburst and quiescence, respectively. The X-ray spectra were analysed and fitted with **XSPEC** version 12.9.1 (Arnaud 1996).

Generally, the X-ray emission from an IP is pulsed at its P . In fact, pulsations of GK Persei in the X-ray band have been detected at $P = 351$ sec both in outbursts and quiescence (e.g. Watson et al. 1985; Norton et al. 1988; Ishida et al. 1992). In the 2015 outburst observation, Zemko et al. (2017) clearly detected the 351 sec pulsation both in the 3–10 keV and 10–79 keV ranges. In the quiescence observation by *NuSTAR*, we detected a faint pulsation with a modulation amplitude of $\sim 10\%$ in the 3–50 keV range. In the present paper, we concentrate on spectral analysis and postpone the study of this pulsation for the next publication.

3 ANALYSIS AND RESULTS

Figure 2 shows 3–50 keV spectra of the outburst and quiescence observations. The background has been subtracted, but the instrumental response has not been removed. Data of FPMA and FPMB are separately plotted. As reported by Zemko et al. (2017) and Suleimanov et al. (2016), the hard X-ray continuum is detected up to 70 keV during the outburst. In quiescence, the source is detected up to 50 keV for the first time. The 3–50 keV count rate of FPMA plus FPMB was 18.09 ± 0.02 count s^{-1} in outburst, and 1.080 ± 0.006 count s^{-1} in quiescence. Thus, the outburst data have 17.5 times higher count rate than those in quiescence. The spectra, particularly the outburst data, exhibit Fe-K line complex at ~ 6.4 keV. From this energy, we regard the lines as mainly of fluorescence origin (from the WD surface and/or the accreting cold matter), rather than ionised lines from the accretion columns.

In the bottom panel, we show the ratio between the two

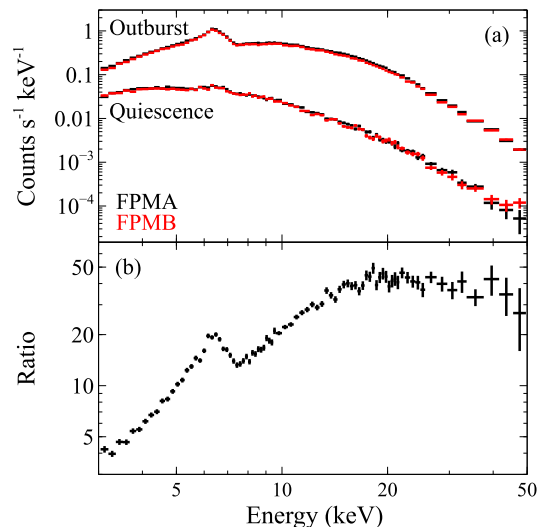


Figure 2. (a) Time averaged FPMA (black) and FPMB (red) spectra of the outburst (brighter) and quiescence (dimmer) observations. (b) Ratios of the FPMA plus FPMB spectra between the two observations.

spectra. It reveals three features of the outburst spectrum, in comparison with that in quiescence. Namely, a stronger low-energy absorption, the stronger Fe-K line, and a continuum break at ~ 20 keV.

To analyse the spectra, we employed a multi-temperature optically-thin plasma model **cemk1** (Done & Osborne 1997) based on a thermal plasma code **mekal** (Mewe et al. 1985, 1986; Liedahl et al. 1995; Kaastra et al. 1996). The differential emission measure of **cemk1** is proportional to the power law function of the plasma temperature T as

$$d(\text{EM}) \propto (T/T_s)^{\alpha-1} dT, \quad (4)$$

where α is a positive parameter. When the accretion column has a cylindrical shape, α is theoretically calculated as 0.43 by Falanga et al. (2005), who used the spectral model computed by Suleimanov et al. (2005). We employed this value because high accretion rate systems such as GK Persei are considered to have nearly cylindrical accretion columns (Hayashi & Ishida 2014a,b). To imitate the reflection effect on the WD surface, **reflect** model (Magdziarz & Zdziarski 1995) was utilised. The solid angle of reflector from the irradiator was set to 2π assuming that the standing shock is formed near the WD surface. The abundances of the **cemk1** and **reflect** components were constrained to be the same assuming that the WD surface near the accretion column is covered by accreted material. A gaussian emission model was also added to represent Fe-K line.

With the model thus constructed, we first fitted the outburst spectrum in the 5–50 keV range, because the **cemk1** model is not available above 50 keV. A partial covering absorption model was applied to the spectral model in addition to a single column absorber. As shown in Figure 3a, this model approximately reproduced the spectrum, but the fit was formally not acceptable under a 90% confidence level, with the reduced chi-squared of $\chi^2/\nu = 2.26$ for 133 degrees of freedom even including 1% systematic error. In fact, as

shown in Figure 3b, significant residuals were seen in the low energy band (<10 keV).

The above fit failure to the outburst spectra is not surprising, because X-ray spectra of IPs are often subject to strong and complex absorption that is not modeled by partial absorption (e.g. Ezuka & Ishida 1999). Since refining the absorption model is beyond the scope of the present paper due to lack of constraining data other than the continuum shape, we have resorted to discarding low-energy ranges until the effects of complex absorption become negligible (see Ezuka & Ishida 1999 for a similar method utilised to avoid complex absorption from affecting the spectral fitting result). By limiting the fit range to 15–50 keV, the fit to the outburst spectrum has become acceptable even with a single column density absorption. The range of T_s constrained in this way, $T_s = 19.4 \pm 0.8$ keV, approximately accommodates the value of $T_s = 17.9$ keV obtained using the 5–50 keV range (though the fit was unacceptable).

The 5–50 keV quiescence spectrum has been reproduced successfully by the spectral model with a single column absorber. Therefore, we have finally conducted a simultaneous fitting using the 15–50 keV band of the outburst spectrum and the 5–50 keV band of the quiescence spectrum. The inclination angle and the abundance were set in common, while the other parameters were allowed to vary independently. This fitting including 1% systematic error has become acceptable with $\chi^2/\nu = 1.01$ for 191 degrees of freedom. The fit result and the best-fit parameters are presented in Figure 3 and Table 2, respectively. Errors are at 90% confidence level. The shock temperature was constrained as $T_s = 19.7^{+1.3}_{-1.0}$ keV in outburst, and $T_s = 36.2^{+3.5}_{-3.2}$ keV in quiescence; thus, T_s was significantly higher in the latter. The 15–50 keV absorbed flux in outburst was 33 times higher than that in quiescence. The 15–50 keV luminosity is also derived as $1.2^{+0.2}_{-0.3} \times 10^{34}$ erg s⁻¹ in outburst, and $3.5^{+0.3}_{-0.5} \times 10^{32}$ erg s⁻¹ in quiescence, with the estimated distance of 477 pc (Harrison et al. 2013a).

For our purpose, we need to calculate the total X-ray flux F which is thought to represent the gravitational energy release from R_{in} to R_{WD} . Starting from the absorbed 15–50 keV flux, F was derived in the following way. First, the absorption and the reflection were removed. Second, the flux above 50 keV was included by extrapolating the best-fit model up to 100 keV. Finally, the contribution below 15 keV was incorporated by integrating the best-fit model down to 0.01 keV. The flux above 100 keV and below 0.01 keV were both estimated to be $\ll 0.01F$. The difference in F between the two spectra amounts to a factor of 65.

Since our final fit to the outburst spectrum was obtained by discarding the data below 15 keV, obviously no information was obtained on the Fe-K line. Hence we fitted the 5–9 keV spectra of the outburst and quiescence to constrain the Fe-K line equivalent width (EW). With a simple model of a single-temperature bremsstrahlung, a gaussian, and a single column absorption model, the EW was measured to be 192 ± 13 eV and 52^{+34}_{-26} eV in outburst and quiescence respectively, as presented in Table 2. The latter is consistent with the value obtained by the 5–50 keV simultaneous fitting.

4 ESTIMATION OF THE WD MASS

As described in Section 1, the accreting matter is considered to be captured by the magnetic field at the inner-radius of the accretion disk R_{in} . In order to estimate the WD mass precisely, R_{in} as well as the shock height h , has to be taken into account. Thus, Equation 1 is modified as

$$kT_s = \frac{3}{8} \mu m_p \frac{GM_{\text{WD}}}{R_{\text{WD}}} \left(\frac{R_{\text{WD}}}{R_{\text{WD}} + h} - \frac{R_{\text{WD}}}{R_{\text{in}}} \right), \quad (5)$$

and therefore T_s is a function of M_{WD} , R_{WD} , h , and R_{in} . At the same time, R_{WD} is related to M_{WD} by the theoretical M – R relation (Equation 2). Employing a numerical calculation of plasma emission in the accretion column, Suleimanov et al. (2008, 2016) theoretically calculated the behaviour of h and T_s , and then reconstructed Equation 5 as the functional form,

$$\frac{kT_s}{1 \text{ keV}} \approx 23.4 \frac{M_{\text{WD}}}{M_{\odot}} \left(1 - 0.59 \frac{M_{\text{WD}}}{M_{\odot}} \right)^{-1} \left(1 - \frac{R_{\text{WD}}}{R_{\text{in}}} \right). \quad (6)$$

Based on the article, this expression is valid for M_{WD} in the range of $0.4 M_{\odot}$ to $1.2 M_{\odot}$. Figure 4 presents, on the M_{WD} v.s. R_{in} plane, contours of T_s implied by Equation 6; in this visualisation, we employed several representative values of T_s , including the present two measurements for outburst and quiescence. Thus, from the quiescence data, we can already set a lower limit as $M_{\text{WD}} > 0.77 M_{\odot}$ (for $R_{\text{in}} \rightarrow \infty$).

The inner-disk radius may be approximately identified as the Alfvén radius, which is determined by an equilibrium between the inward gravity and the outward magnetic pressure. Assuming spherical accretion and dipole magnetic field, Elsner & Lamb (1977) described it as

$$\frac{R_{\text{in}}}{R_{\text{WD}}} \approx 2.3 \left(\frac{\dot{M}}{10^{20} \text{ g/s}} \right)^{-2/7} \left(\frac{M_{\text{WD}}}{M_{\odot}} \right)^{-1/7} \left(\frac{R_{\text{WD}}}{10^9 \text{ cm}} \right)^{5/7} \left(\frac{B}{10^6 \text{ G}} \right)^{4/7}, \quad (7)$$

where \dot{M} is the accretion rate and B is again the dipole magnetic-field strength on the WD surface. An extension of this formalism by Ghosh & Lamb (1979) has been shown to give a good explanation to the accretion-induced spin period changes in the binary X-ray pulsar 4U 1626–67 (Takagi et al. 2016). Since mass accretion that takes place in GK Persei shares similar geometry outside R_{in} , this formalism is employed here. With this formalisation, R_{in} thus shrinks as \dot{M} increases, T_s must be lower in outbursts than in quiescence, in agreement with our result. Systematic uncertainties associated with this equation are discussed in Section 5.4.3.

In order to utilise our two observations in equal manner, let us introduce the ratio γ between the two R_{in} values as

$$\gamma = \frac{R_{\text{in}}^{\text{qui}}}{R_{\text{in}}^{\text{out}}} = \left(\frac{\dot{M}^{\text{out}}}{\dot{M}^{\text{qui}}} \right)^{-2/7}, \quad (8)$$

where the superscripts “out” and “qui” indicate the outburst and quiescence values, respectively. Since \dot{M} can be related to the total X-ray luminosity L as

$$\dot{M} = L \times \left[\frac{GM_{\text{WD}}}{R_{\text{WD}}} \left(1 - \frac{R_{\text{WD}}}{R_{\text{in}}} \right) \right]^{-1}, \quad (9)$$

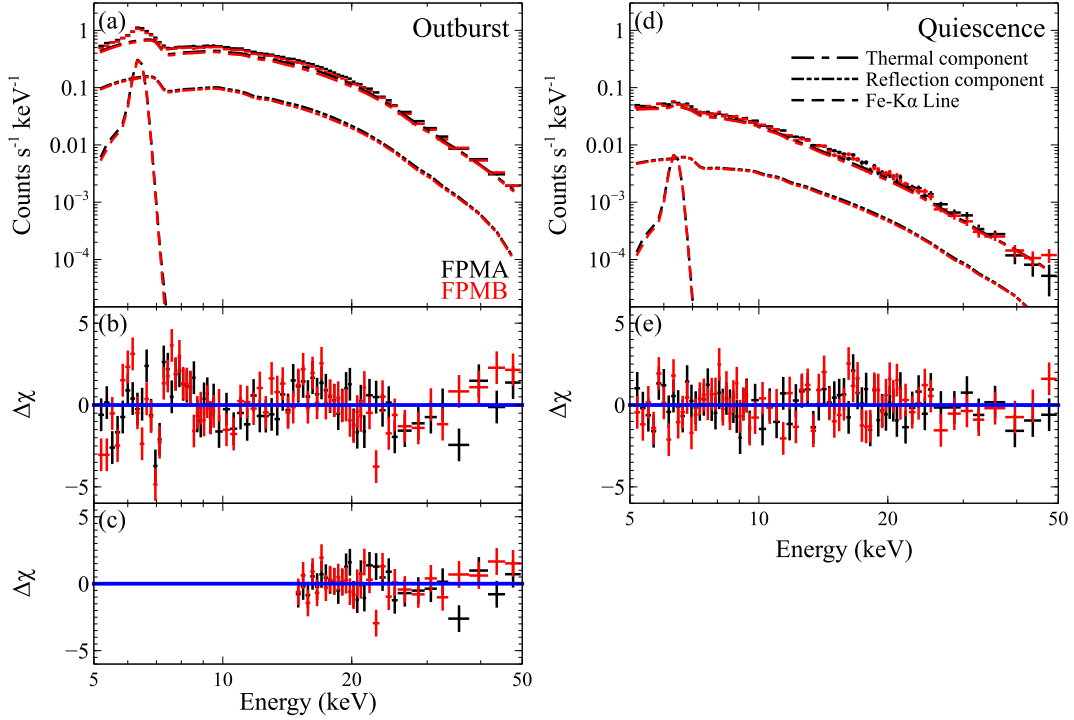


Figure 3. (a) The *NuSTAR* FPMA (black) and FPMB (red) spectra in outburst, and their best-fit models with a partial covering absorption. The thermal component, reflection component, and Fe-K line are indicated by the dash-dot, dash-dot-dot, and dashed lines, respectively. (b) The residuals from the 5–50 keV fit in panel (a). (c) The residuals of the 15–50 keV fit. (d) The quiescence spectrum and its best-fit model. (e) The residuals of the fit in panel (d).

Table 2. Best-fit parameters of the multi temperature plasma emission and reflection model to the time-averaged spectra.

	N_{H}^{a} 10^{22} cm^{-2}	$\cos i^{\text{b}}$	T_{s}^{c} keV	Z^{d} Z_{\odot}	EW^{e} eV	EW^{f} eV	F_{15-50}^{g} $\text{erg cm}^{-2} \text{ s}^{-1}$	$F_{0.01-100}^{\text{h}}$ $\text{erg cm}^{-2} \text{ s}^{-1}$	χ^2/ν
Outburst	124^{+14}_{-12}	<0.22	$19.7^{+1.3}_{-1.0}$	0.10 ± 0.04	–	192 ± 13	$4.3^{+0.6}_{-0.9} \times 10^{-10}$	$3.6^{+0.5}_{-0.8} \times 10^{-9}$	1.01
Quiescence	10^{+3}_{-4}		$36.2^{+3.5}_{-3.2}$		55^{+34}_{-6}	52^{+34}_{-26}	$1.3^{+0.1}_{-0.2} \times 10^{-11}$	$5.5^{+0.5}_{-0.9} \times 10^{-11}$	

^a Column density of the single-column absorption.

^b Cosine of the inclination angle between the reflection surface and the observer’s line-of-sight.

^c The highest temperature of the accretion column.

^d Abundance relative to Solar.

^e Equivalent width of the Fe-K line by the 5–50 keV wide band fit.

^f Equivalent width of the Fe-K line by the 5–9 keV narrow band fit.

^g Obtained model fluxes in the 15–50 keV band.

^h Extrapolated total X-ray fluxes in the 0.01–100 keV band.

we can combine Equation 6, 8, and 9 to obtain

$$\gamma = \left(\frac{L^{\text{qui}} \times T_{\text{s}}^{\text{out}}}{L^{\text{out}} \times T_{\text{s}}^{\text{qui}}} \right)^{-2/7} = \left(\frac{F^{\text{qui}} \times T_{\text{s}}^{\text{out}}}{F^{\text{out}} \times T_{\text{s}}^{\text{qui}}} \right)^{-2/7}, \quad (10)$$

where F is the total X-ray flux. Then, the values of T_{s} and F measured in the two observations (Table 2) yield, via Equation 8,

$$\gamma = 3.9 \pm 0.5. \quad (11)$$

We can now determine the value of M_{WD} in Figure 4 so that the two R_{in} values satisfy equation 11 as indicated by a pair of horizontal lines in Figure 4; $R_{\text{in}}^{\text{out}} = 1.9^{+0.4}_{-0.2} R_{\text{WD}}$,

$R_{\text{in}}^{\text{qui}} = 7.4^{+2.1}_{-1.2} R_{\text{WD}}$, and $M_{\text{WD}} = 0.87 \pm 0.05 M_{\odot}$ are yielded with $R_{\text{WD}} = (6.6 \pm 0.4) \times 10^8 \text{ cm}$. The obtained $R_{\text{in}}^{\text{qui}}$ and $R_{\text{in}}^{\text{out}}$ satisfy the accretion condition $R_{\text{in}} < R_{\Omega} \sim 11 R_{\text{WD}}$ with $P = 351 \text{ sec}$, $M_{\text{WD}} = 0.87 M_{\odot}$, and Equation 3. Thus, the clear increase in T_{s} , observed in the transition from outburst to quiescence (Table 2), has been successfully explained as a factor $\gamma \sim 4$ increase in R_{in} , in response to the decrease in \dot{M} by a factor of 120: \dot{M} is obtained from Equation 9 and F as $\dot{M}^{\text{out}} = (1.2 \pm 0.4) \times 10^{18} \text{ g s}^{-1}$ and $\dot{M}^{\text{qui}} = (1.0 \pm 0.3) \times 10^{16} \text{ g s}^{-1}$, respectively. An advantage of this method is that any systematic uncertainty involved in the coefficient of Equation 7 cancels by taking the ra-

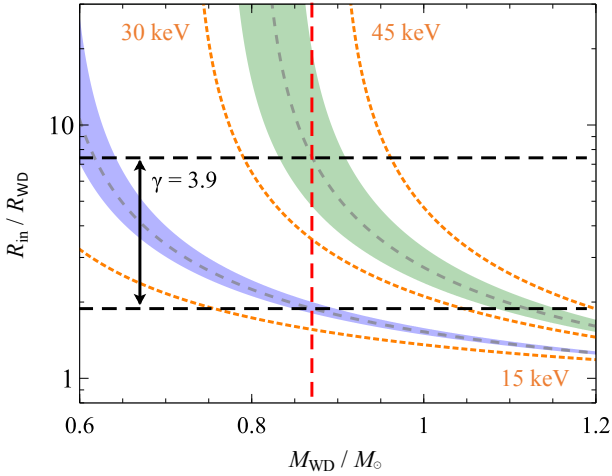


Figure 4. Contours (dotted orange curves) of T_s given by Equation 6, shown on the M_{WD}/M_{\odot} – $R_{\text{in}}/R_{\text{WD}}$ plane. Allowed regions for T_s in outburst and quiescence are indicated by blue and green, respectively. The dashed red line (vertical) shows a value of M_{WD} that satisfies $\gamma = 3.9$ between the two measurements.

tio of the two equations (Equation 10). Further discussion continues in Section 5.4.3.

5 DISCUSSION

5.1 Comparison between the Two Observations

In the present paper, we analysed a pair of *NuSTAR* spectra of GK Persei acquired in 2015. In the 5 months from the outburst observation on April 4 to the quiescence one on September 8, the optical emission from GK Persei diminished by ~ 3.2 magnitude or ~ 19 times (Figure 1). Meanwhile, the 3–50 keV FPMA+FPMB count rate decreased by a factor of 17, and the absorbed 15–50 keV flux by a factor of 33. The two factors become different because the outburst spectrum is more absorbed (Figure 2), and hence the count rate which is more weighted towards lower energies changed less than that of the flux which is more weighted towards higher energies. Correcting these spectra for the respective absorption, and extrapolating the best-fit models to >50 keV and <15 keV, the 0.01–100 keV unabsorbed total X-ray flux is inferred to have changed by 65 times.

In addition to the changes in the X-ray flux and absorption, we detected a clear increase in T_s from the outburst (~ 20 keV) to the quiescence (~ 36 keV) observations. Employing the disk-magnetosphere interaction model of Ghosh & Lamb (1979), the change in T_s has successfully been interpreted as due to a factor ~ 4 change in R_{in} , in a negative correlation with \dot{M} . Considering that the gravitational potential drop available for the X-ray emission (from R_{in} to R_{WD}) thus became deeper in quiescence, the total X-ray luminosity change has been converted to a factor of 120 difference in \dot{M} . For reference, the temperature change we observed is qualitatively consistent with the report by Zemko et al. (2017), that the *Swift*/XRT light curve of the hardness ratio indicated a temperature decrease as the outburst proceeded

towards its peak, and the very high value of T_s measured by Yuasa et al. (2016) at the outburst onset.

As presented in Table 2, the EW of the Fe-K line (nearly neutral component) was ~ 4 times higher in outburst. The line is usually ascribed to two emitting sources: the ambient matter as represented by \dot{M} and N_{H} , and the WD surface as represented by reflection. Evidently, both \dot{M} and N_{H} were higher in outburst, so that the Fe-K line EW from the first source must be higher as well. Furthermore, as discussed later in Section 5.4.2, the standing shock is considered to come closer to the surface when \dot{M} increases, because the higher density would increase the volume emissivity in the accretion columns and higher shock temperature can be dissipated within the boundary conditions. This will in turn increase the solid angle of reflection, and yield a high EW from the second source. The higher EW observed in outburst may be explained qualitatively as a combination of these two effects.

5.2 Comparison with Previous Optical Results

The WD mass we obtained, $M_{\text{WD}} = 0.87 \pm 0.05 M_{\odot}$, is consistent with the optical results ($\geq 0.78 M_{\odot}$: Reinsch 1994, $\geq 0.63 M_{\odot}$: Morales-Rueda et al. 2002). These optical estimates gave only lower limits of M_{WD} because eclipses of the WD do not occur in the GK Persei system, and hence the inclination angle remains poorly constrained. In contrast, our method with X-rays can estimate M_{WD} without the knowledge of the inclination angle. When our M_{WD} determination is combined with the ratio of the WD mass and the companion mass $M_{\text{K}}/M_{\text{WD}} = 0.55 \pm 0.21$, and the optically determined mass function

$$\frac{M_{\text{WD}}}{M_{\odot}} \frac{\sin^3 i}{(1 + M_{\text{K}}/M_{\text{WD}})^2} = 0.362 \quad (12)$$

(Morales-Rueda et al. 2002), the companion mass is constrained as $M_{\text{K}} = 0.48 \pm 0.18 M_{\odot}$, and then the lower limit of the inclination angle is derived as $i \geq 63^\circ$. This lower limit on i is consistent with the optical upper limit, $i \leq 73^\circ$, required by the lack of eclipses. Combining these results, $63^\circ \leq i \leq 73^\circ$ is obtained.

5.3 Comparison with Previous X-ray Results

Let us revisit the past X-ray result with the PCA and HEXTE onboard *RXTE*, obtained during an outburst by Suleimanov et al. (2005). They measured $T_s = 21 \pm 3$ keV, and derived $M_{\text{WD}} = 0.59 \pm 0.05 M_{\odot}$ assuming $R_{\text{in}} \gg R_{\text{WD}}$ (the author noted that M_{WD} would be underestimated). At that time, the total X-ray flux in the 0.1–100.0 keV range was measured to be 8.86×10^{-10} erg cm $^{-2}$ s $^{-1}$. When we use the present *cemekl* model of the same T_s , the 0.01–100 keV flux is re-estimated as 1.0×10^{-9} erg cm $^{-2}$ s $^{-1}$, which falls in between the present two measurements (Table 2). Then, compared with them, the value of R_{in} during the *RXTE* observation is estimated, from Equation 8, as $R_{\text{in}} \simeq 1.5 R_{\text{in}}^{\text{out}} \simeq 0.37 R_{\text{in}}^{\text{qui}} \simeq 2.8 R_{\text{WD}}$. Substituting this value and $T_s = 21$ keV into Equation 6, or equivalently referring to Figure 4, $M_{\text{WD}} \sim 0.8 M_{\odot}$ is derived. This revised mass is probably consistent with our result when various errors are taken in account. Our result is also consistent with the mass

estimation $M_{\text{WD}} = 0.90 \pm 0.12 M_{\odot}$ by [Brunschweiler et al. \(2009\)](#) with *Swift*/BAT within errors, as already referred to in Section 1.

The present outburst data were already analysed by [Zemko et al. \(2017\)](#). They derived $T_s = 16.2^{+0.5}_{-0.4}$ keV by the 3–50 keV broad band fitting, wherein the *NuSTAR* data are combined with those from the *Chandra* MEG and HETG. Their T_s value is $\sim 18\%$ lower than our outburst result. This discrepancy may be caused by difference of emission models. The `mkcflow` model they employed is a superposition of the `mekal` thermal emission model, like the `cemekl` model we used, but the emission measure of `mkcflow` is weighted by the inverse of the bolometric luminosity at each temperature T . Because the bolometric flux is $\propto T^{1/2}$ when only the bremsstrahlung continuum is considered, the differential emission measure becomes $\propto (T/T_s)^{-1/2}$, and $\alpha = 0.5$ by Equation 4. It is slightly different from that of `cemekl`, $\alpha = 0.43$, and will make the composite spectrum more weighted towards higher temperatures. In the fit by [Zemko et al. \(2017\)](#), this effect is considered to be compensated by the lower T_s . (In the relevant temperature range, α would not change very much even considering the lines.)

[Suleimanov et al. \(2016\)](#) also analysed the same outburst data and obtained $M_{\text{WD}} = 0.86 \pm 0.02 M_{\text{WD}}$. This is fully consistent with our estimate. In deriving this result, however, they employed a method that differs from ours in two points: T_s and R_{in} . They fitted the 20–70 keV spectrum in outburst with their newly calculated spectral model (PSR model), and obtained $T_s \sim 26.3$ keV. They also employed, for an illustrative purpose, a single temperature bremsstrahlung model and obtained its temperature as 16.7 ± 0.2 keV; via Equation 2 in [Suleimanov et al. \(2016\)](#), this was converted to a consistent shock temperature of $T_s = 26.0 \pm 0.3$ keV. For consistency, we fitted the 20–70 keV spectrum with the bremsstrahlung model, and obtained the temperature as 16.6 ± 0.3 keV. Therefore, the present data analysis is consistent with theirs. They also derived $R_{\text{in}} = 2.8 \pm 0.2 R_{\text{WD}}$ by the power density spectral analysis ([Revnivtsev et al. 2009](#)). After all, their T_s is 1.3 times higher than our T_s , and their R_{in} is 1.5 times larger than ours. These differences in T_s and R_{in} happened to cancel out, to yield the two M_{WD} estimates which are very close to each other.

5.4 Systematic Uncertainties of the Mass Estimation

So far, we considered only statistic errors. Here, let us evaluate possible systematic errors that can affect our result.

5.4.1 Emission Models of the Accretion Column

In the present paper, we assumed the accretion columns to have a cylindrical shape, and hence employed the `cemekl` model with $\alpha = 0.43$ in Equation 4. Recently, emission models with a dipole geometry for the accretion column have been developed, including ACRAD model by [Hayashi & Ishida \(2014a,b\)](#), and the PSR model by [Suleimanov et al. \(2016\)](#). We thus refitted the spectra with the PSR model (`ipolar` model in XSPEC). The energy range below 7 keV in quiescence was ignored in this analysis because `ipolar` model has abundances fixed to $1 Z_{\odot}$ and cannot reproduce

the Fe emission lines which are well described with sub-solar Fe abundance. The shock temperature was then obtained as 20.4 ± 0.6 keV in outburst and $37.3^{+3.9}_{-3.3}$ keV in quiescence, and the WD mass was constrained as $M_{\text{WD}} = 0.88 \pm 0.05 M_{\odot}$. All these values agree well with the results in Section 3 within the statistic errors. Therefore, we consider that slight differences of the emission models, namely the detailed morphological and emissivity structures of the post-shock region, have insignificant impact on the mass estimation method presented above, at least, when applied to GK Persei.

5.4.2 Shock Height

As presented in Equation 5, T_s depends on the shock height h , which is thought to negatively correlate with \dot{M} . This effect was theoretically calculated and incorporated in Equation 6. However, even if the effect of h is ignored (i.e. $h = 0$), the value of M_{WD} changes by less than 0.5%, which is much smaller than the statistic error. Therefore, the value of h itself would not affect the WD mass estimation in GK Persei.

In our spectral analysis, the reflection model was included to represent the reflection effect on the WD surface. The solid angle of the reflection was fixed to 2π simply assuming that the shock heating occurs just above the WD surface. In reality, h are calculated as $0.014 R_{\text{WD}}$ and $0.026 R_{\text{WD}}$ by Equation 5, corresponding to the solid angle of 1.8π and 1.7π in outburst and quiescence, respectively. We thus repeated the spectral fitting using these solid angles, to find that neither T_s^{out} nor T_s^{qui} changes by more than 0.2%. Therefore, the result of M_{WD} is not affected either.

5.4.3 Alfvén Radius

As expressed by Equation 7, we assumed that R_{in} is equal to the Alfvén radius. This formalism by [Elsner & Lamb \(1977\)](#), which considers spherical accretion, includes two possible uncertainties. One is the coefficient of Equation 7. In the case of disk accretion in rotating magnetic neutron star systems, [Ghosh & Lamb \(1979\)](#) argued that the actual inner-disk radius is almost half the Alfvén radius. Therefore, the estimated values of R_{in} are probably subject to an uncertainty by a constant factor. However, this uncertainty cancels out in our work by taking the ratio $\gamma = R_{\text{in}}^{\text{qui}}/R_{\text{in}}^{\text{out}}$. Hence, our M_{WD} estimation is free from the uncertainty, because in Figure 4 we utilise γ rather than the actual values of R_{in} .

The other uncertainty is the power law index Γ of \dot{M} in Equations 7, 8, and 10, for which we employ $\Gamma = -2/7$. A recent 3D simulation of accretion flows around a neutron star yields $\Gamma = -1/5$ ([Kulkarni & Romanova 2013](#)). In addition, [Suleimanov et al. \(2016\)](#) observationally evaluated $\Gamma = -0.2^{+1.0}_{-1.5}$. We thus quote a systematic uncertainty by $\Delta\Gamma \sim 0.1$, which translates into $\sim 7\%$ systematic errors in M_{WD} .

Adding up all these uncertainties, the overall systematic error in the WD mass estimate becomes comparable to the statistical error. Including this in quadrature, we quote our final mass determination as $M_{\text{WD}} = 0.87 \pm 0.08 M_{\odot}$, with $R_{\text{WD}} = (6.6 \pm 0.6) \times 10^8$ cm.

5.5 Strength of Magnetic Field on WD Surface

Since M_{WD} , R_{WD} , and R_{in} were determined, the strength of the magnetic field on the WD surface can be now estimated to be $B \sim 5 \times 10^5$ G using Equation 7 and the distance of the object 477 pc (Harrison et al. 2013a). This value is consistent with the typical magnetic field strength of IPs. However, unlike M_{WD} , this result is subject to the uncertainties discussed in Section 5.4.3. If the coefficient of Equation 7 has an uncertainty by a factor of 2 for example, B changes by a factor of 3–4.

Magnetic field measurements of Polars and strongly magnetised IPs ($\sim 10^7$ G) have been made by detecting spin-modulated polarisation in the near-ultraviolet to near-infrared bands (e.g. Pirola et al. 2008). However, the magnetic field of $\sim 10^5$ G on the WD surface cannot be measured at present. Therefore, the present method provides the only way to measure relatively weak magnetic field of IPs, even though it has a relatively poor accuracy due to the above-mentioned model uncertainty.

6 CONCLUSION

Analysing the outburst and quiescence data of GK Per obtained with *NuSTAR*, we found the 0.01–100 keV unabsorbed flux was $3.6^{+0.5}_{-0.8} \times 10^{-9}$ erg s $^{-1}$ cm $^{-2}$ and $5.5^{+0.5}_{-0.9} \times 10^{-11}$ erg s $^{-1}$ cm $^{-2}$, respectively, with a factor 65 difference. Analysing the 5–50 keV or 15–50 keV spectra using a multi-temperature spectral model, the shock temperature was determined as 19.7 $^{+1.3}_{-1.0}$ keV in outburst, and 36.2 $^{+3.5}_{-3.2}$ keV in quiescence. Assuming that this temperature difference is caused by a compression of the magnetosphere and the associated change in R_{in} , we determined the WD mass in GK Per as $M_{\text{WD}} = 0.87 \pm 0.08 M_{\odot}$, together with the radius as $R_{\text{WD}} = (6.6 \pm 0.6) \times 10^8$ cm (including a 7% systematic error). The values of R_{in} , relative to R_{WD} , was derived as $R_{\text{in}}/R_{\text{WD}} = 1.9^{+0.4}_{-0.2}$ in outburst and $R_{\text{in}}/R_{\text{WD}} = 7.4^{+2.1}_{-1.2}$ in quiescence, and the mass accretion rate is estimated to have changed by a factor of 120 between the two observations. Combined with optical observations, the inclination angle of GK Per is tightly constrained as $63^{\circ} \leq i \leq 73^{\circ}$. We also estimated the magnetic field of the WD as $\sim 5 \times 10^5$ G although it is subject to large systematic error uncertainty. The overall results demonstrate the power of our mass determination method using X-ray luminosity changes, wherein some major systematic uncertainties cancel out.

ACKNOWLEDGEMENTS

This work was made use of data obtained with the *NuSTAR* mission, and softwares obtained from the High Energy Astrophysics Science Archive Research Center at NASA Goddard Space Center. The authors also acknowledge the use of X-ray monitoring data provided by *Swift* data archive, and optical data from *AAVSO International Database* contributed by observers worldwide. Y.W. is supported by the Junior Research Associate Programme in RIKEN.

REFERENCES

- Aizu K., 1973, *Progress of Theoretical Physics*, **49**, 1184
 Arnaud K. A., 1996, in Jacoby G. H., Barnes J., eds, *Astronomical Society of the Pacific Conference Series Vol. 101, Astronomical Data Analysis Software and Systems V*. p. 17
 Brunschweiler J., Greiner J., Ajello M., Osborne J., 2009, *A&A*, **496**, 121
 Cropper M., Ramsay G., Wu K., 1998, *MNRAS*, **293**, 222
 Done C., Osborne J. P., 1997, *MNRAS*, **288**, 649
 Elsner R. F., Lamb F. K., 1977, *ApJ*, **215**, 897
 Ezuka H., Ishida M., 1999, *ApJS*, **120**, 277
 Falanga M., Bonnet-Bidaud J. M., Suleimanov V., 2005, *A&A*, **444**, 561
 Fujimoto R., Ishida M., 1997, *ApJ*, **474**, 774
 Ghosh P., Lamb F. K., 1979, *ApJ*, **234**, 296
 Hachisu I., Kato M., 2007, *ApJ*, **662**, 552
 Hale G. E., 1901, *ApJ*, **13**
 Harrison T. E., Bornak J., McArthur B. E., Benedict G. F., 2013a, *ApJ*, **767**, 7
 Harrison F. A., et al., 2013b, *ApJ*, **770**, 103
 Hayashi T., Ishida M., 2014a, *MNRAS*, **438**, 2267
 Hayashi T., Ishida M., 2014b, *MNRAS*, **441**, 3718
 Ishida M., Sakao T., Makishima K., Ohashi T., Watson M. G., Norton A. J., Kawada M., Koyama K., 1992, *MNRAS*, **254**, 647
 Kaastra J. S., Mewe R., Nieuwenhuijzen H., 1996, in Yamashita K., Watanabe T., eds, *UV and X-ray Spectroscopy of Astrophysical and Laboratory Plasmas*. pp 411–414
 Krimm H. A., et al., 2013, *ApJS*, **209**, 14
 Kulkarni A. K., Romanova M. M., 2013, *MNRAS*, **433**, 3048
 Liedahl D. A., Osterheld A. L., Goldstein W. H., 1995, *ApJ*, **438**, L115
 Magdziarz P., Zdziarski A. A., 1995, *MNRAS*, **273**, 837
 Mewe R., Gronenschild E. H. B. M., van den Oord G. H. J., 1985, *A&AS*, **62**, 197
 Mewe R., Lemen J. R., van den Oord G. H. J., 1986, *A&AS*, **65**, 511
 Morales-Rueda L., Still M. D., Roche P., Wood J. H., Lockley J. J., 2002, *MNRAS*, **329**, 597
 Nauenberg M., 1972, *ApJ*, **175**, 417
 Norton A. J., Watson M. G., King A. R., 1988, *MNRAS*, **231**, 783
 Pirola V., Vornanen T., Berdyugin A., Coyne G. V., J. S., 2008, *ApJ*, **684**, 558
 Reinsch K., 1994, *A&A*, **281**, 108
 Revnivtsev M., Churazov E., Postnov K., Tsygankov S., 2009, *A&A*, **507**, 1211
 Suleimanov V., Revnivtsev M., Ritter H., 2005, *A&A*, **435**, 191
 Suleimanov V., Poutanen J., Falanga M., Werner K., 2008, *A&A*, **491**, 525
 Suleimanov V., Doroshenko V., Ducci L., Zhukov G. V., Werner K., 2016, *A&A*, **591**, A35
 Takagi T., Mihara T., Sugizaki M., Makishima K., Morii M., 2016, *PASJ*, **68**, S13
 Warner B., 1995, *Cambridge Astrophysics Series*, **28**
 Watson M. G., King A. R., Osborne J., 1985, *MNRAS*, **212**, 917
 Wilber A., Neric M., Starrfield S., Wagner R. M., Woodward C. E., 2015, *The Astronomer's Telegram*, **7217**
 Williams A. S., 1901, *MNRAS*, **61**, 337
 Yuasa T., Nakazawa K., Makishima K., Saitou K., Ishida M., Ebisawa K., Mori H., Yamada S., 2010, *A&A*, **520**, A25
 Yuasa T., Hayashi T., Ishida M., 2016, *MNRAS*, **459**, 779
 Zemko P., Orio M., Luna G. J. M., Mukai K., Evans P. A., Bianchini A., 2017, *MNRAS*, **469**, 476
 Šimon V., 2002, *A&A*, **382**, 910

This paper has been typeset from a $\text{\TeX}/\text{\LaTeX}$ file prepared by the author.